Laser cooling of transition-metal atoms

Scott Eustice,[1,2,*] Kayleigh Cassella[1,3] and Dan Stamper-Kurn[1,2,4,†]

[1]*Department of Physics, University of California, Berkeley, California 94720, USA*
[2]*Challenge Institute for Quantum Computation, University of California, Berkeley, California 94720, USA*
[3]*Atom Computing Inc., Berkeley, California 94710, USA*
[4]*Materials Sciences Division, Lawrence Berkeley National Laboratory, Berkeley, California 94720, USA*

We propose the application of laser cooling to a number of transition-metal atoms, allowing numerous bosonic and fermionic atomic gases to be cooled to ultralow temperatures. The nonzero electron orbital angular momentum of these atoms implies that strongly atom-state-dependent light-atom interactions occur even for light that is far-detuned from atomic transitions. At the same time, many transition-metal atoms have small magnetic dipole moments in their low-energy states, reducing the rate of dipolar-relaxation collisions. Altogether, these features provide compelling opportunities for future ultracold-atom research. Focusing on the case of atomic titanium, we identify the metastable $a\,^5F_5$ state as supporting a $J \to J + 1$ optical transition with properties similar to the D_2 transition of alkali-metal atoms, and suited for laser cooling. The high total angular momentum and electron spin of this state suppresses leakage out of the nearly closed optical transition to a branching ratio estimated below $\sim 10^{-5}$. Following the pattern exemplified by titanium, we identify optical transitions that are suited for laser cooling of elements in the scandium group (Sc, Y, La), the titanium group (Ti, Zr), the vanadium group (V, Nb), the manganese group (Mn, Tc), and the iron group (Fe, Ru).

I. INTRODUCTION

Laser cooling and the achievement of quantum degeneracy of atomic gases has led to an ever broadening range of scientific investigations and applications. This growing impact on science and technology has been fueled by the availability of quantum gases produced from an increasing number of elements, each of which has a different set of properties that can enable a family of experiments. For example, the fortuitous collisional properties of rubidium and sodium enabled the first realizations of scalar [1,2] and spinor [3–5] atomic Bose-Einstein condensation. The accessible Feshbach resonances of lithium allowed studies of Efimov states [6]. Isotopes of potassium and lithium allowed the study of resonantly interacting Fermi gases [7–10]. The detectability of single metastable helium atoms on microchannel plate detectors allowed for studies of quantum atom optics [11]. The narrow lines of alkaline-earth-metal atoms and ytterbium enabled the realization of optical lattice clocks [12,13]. The magnetism of chromium allowed for studies of quantum ferrofluids [14], accentuated by the even stronger magnetic dipole interactions of dysprosium [15] and erbium [16]. Gaining access to a greater variety of ultracold atomic gases can, therefore, be expected to broaden the impact of ultracold atomic physics even further.

Conversely, the limitations of present-day ultracold atom systems pose limitations on the range of scientific topics that they can be used to study. As an example, we consider the prospect of studying gases in a stable mixture of internal spin states while they are subject also to coherent spin-state-dependent optical potentials. Each of these two conditions can be achieved separately in extant quantum gases: Stable spinor gases are realized with alkali-metal atoms, whose small magnetic moments forestall inelastic dipolar relaxation collisions [17]. Highly coherent spin-dependent optical potentials are realized for lanthanide atoms, owing to their complex atomic structures [18]. However, in neither case are *both* conditions simultaneously achieved: Spin-dependent optical potentials for alkali-metal atoms have low coherence (as we explain in Sec. II). Spinor gases of lanthanide atoms decay generally through strong magnetic dipolar relaxation, although the specific relaxation via collision channels with indistinguishable initial or final spin states can be suppressed by Fermi statistics [19].

Here, we describe pathways for laser cooling a number of transition-metal elements, including those in the scandium group (Sc, Y, La), the titanium group (Ti, Zr, and possibly Hf), the vanadium group (V, Nb), the manganese group (Mn, Tc), and the iron group (Fe, Ru, and possibly Os). Specifically, we find for all these elements that there is a strong, electric-dipole allowed, optical transition (see Table I), with linewidth on the order of 10 MHz, which resembles the D_2 line of alkali-metal atoms in that an electron is driven from $ns_{1/2}$ to the $np_{3/2}$ state. The lower level on this transition, which we call the laser-cooling state, is either the atomic ground state (in Ru and Mn) or a metastable excited state (in the other cases). In all cases, these transitions are cycling, or at least very nearly so, and connect states with total angular momentum $J \to J + 1$.

*scott_eustice@berkeley.edu
†dmsk@berkeley.edu

TABLE I. Laser-cooling lines of transition metals. Configurations, terms, and essential cooling line information is summarized. Values with an asterisk indicate that the wavelength has been inferred from energy-level data, not measured directly. All values are drawn from the NIST database [30].

Atom	Ground state		Metastable state		Excited state		Cooling trans. (nm)	Linewidth (MHz/2π)
	Config.	Term	Config.	Term	Config.	Term		
Sc	$3d4s^2$	$a\,^2D_{3/2}$	$3d^2(^3F)4s$	$a\,^4F_{9/2}$	$3d^2(^3F)4p$	$z\,^4G^\circ_{11/2}$	567	8.6
Y	$4d5s^2$	$a\,^2D_{3/2}$	$4d^2(^3F)5s$	$a\,^4F_{9/2}$	$4d^2(^3F)5p$	$z\,^4G^\circ_{11/2}$	547	10.0
La	$5d6s^2$	$^2D_{3/2}$	$5d^2(^3F)6s$	$^4F_{9/2}$	$5d^2(^3F)6p$	$^4G^\circ_{11/2}$	625	5.86
					$4f5d(^3G^\circ)6s$	$^4G^\circ_{11/2}$	406	8.9
Ti	$3d^24s^2$	$a\,^3F_4$	$3d^3(^4F)4s$	$a\,^5F_5$	$3d^3(^4F)4p$	$y\,^5G^\circ_6$	498	10.5
					$3d^2(^3F)4s4p(^3P^\circ)$	$z\,^5G^\circ_6$	1040	0.0113
Zr	$4d^25s^2$	$a\,^3F_4$	$4d^3(^4F)5s$	$a\,^5F_5$	$4d^3(^4F)5p$	$y\,^5G^\circ_6$	469	
					$4d^2(^3F)5s5p(^3P^\circ)$	$z\,^5G^\circ_6$	902*	
V	$3d^34s^2$	$a\,^4F_{3/2}$	$3d^4(^3H)4s$	$a\,^4H_{13/2}$	$3d^4(^3H)4p$	$z\,^4I^\circ_{15/2}$	445	13.0
Nb	$4d^4(^5D)5s$	$a\,^6D_{1/2}$	$4d^4(^3H)5s$	$a\,^4H_{13/2}$	$4d^4(^3H)5p$	$z\,^4I^\circ_{15/2}$	413	
					$4d^35s(^3H)5p$	$^4I^\circ_{15/2}$	463	
Mn	$3d^54s^2$	$a\,^6S_{5/2}$			$3d^5(^6S)4s4p(^3P^\circ)$	$z\,^6P^\circ_{7/2}$	403	2.71
			$3d^6(^3H)4s$	$a\,^4H_{13/2}$	$3d^6(^3H)4p$	$z\,^4I^\circ_{15/2}$	405*	
Tc	$4d^55s^2$	$a\,^6S_{5/2}$	$4d^6(^3H)5s$	$^4H_{13/2}$	$4d^6(^3H)5p$	$^4I^\circ_{15/2}$	378	
Fe	$3d^64s^2$	$a\,^5D_4$	$3d^7(^4F)4s$	$a\,^5F_5$	$3d^7(^4F)4p$	$z\,^5G^\circ_6$	358	16.2
Ru	$4d^7(^4F)5s$	$a\,^5F_5$			$4d^7(^4F)5p$	$z\,^5G^\circ_6$	350	13.7

As such, these transitions are suitable for standard laser-cooling techniques such as Zeeman slowing [21], magneto-optical trapping [22], and polarization-gradient cooling [23,24].

These elements have atomic properties that differ from those of existing ultracold atomic gases. Present-day quantum gases can be divided into two categories: spherical atoms and highly nonspherical atoms. Specifically, in the spherical-atom category we include alkali-metal atoms, alkaline-earth-metal atoms, metastable noble gases, and additional filled-shell (Yb) or half-filled-shell (Cr) atoms, for which the total orbital electronic angular momentum in the ground state is $L = 0$. In the category of highly nonspherical atoms we identify the lanthanide atoms that have been laser cooled [25–27] and brought to quantum degeneracy [15,16]. For these atoms, the ground-level electronic angular momentum is large, e.g., $L = 6$ for Dy and $L = 5$ for Er.

The transition-metal elements identified in this work have properties that are intermediate to these two categories. For all these elements, both the laser-cooling state and, with the exception of Mn and Tc, also the ground state have $L \neq 0$. As we discuss below, as for the lanthanide atoms, this condition leads to highly coherent anisotropic light-atom interactions with far-off-resonant light. However, because the orbital angular momentum of these transition-metal elements is smaller than that of lanthanide elements, we expect ultracold collisions to be more similar to those of spherical atoms. Specifically, we expect ultracold spinor gases formed of many of these atoms to be stable against inelastic dipolar relaxation collisions. Altogether, following previous examples, we expect the addition of this family of transition-metal elements to the rank of ultracold atomic gases will enable developments in ultracold atomic (and also molecular) physics.

This paper is organized as follows. In Sec. II, we illustrate our proposed laser-cooling scheme by focusing deeply on the example of atomic titanium. Through this example, we explain how the laser-cooling level is identified as a highly spin-polarized configuration with a single electron in the valence s orbital. The case of titanium also exemplifies experimental techniques required to work with ultracold transition-metal atoms, and points to several potential scientific uses for quantum-degenerate transition-metal atomic gases. In Sec. III, we describe laser-cooling pathways for other atoms in the titanium group and in the iron group, which are all similar to the case of titanium. These include atomic iron, for which laser cooling has already been demonstrated [28] by the approach described in this paper. We conclude in Sec. IV by describing briefly the opportunities for laser-cooling atoms in the scandium, vanadium, and manganese groups.

II. TITANIUM AND ITS COMPARISON TO EXISTING QUANTUM GASES

Atomic titanium (Ti) has four valence electrons surrounding a closed-shell core. In its lowest-energy term $a\,^3F$, Ti has an "alkaline-earth-metal-like" configuration $3d^24s^2$. This level is split by fine structure into states with total angular momentum $J = 2$, 3, and 4, with the $a\,^3F_2$ state being the overall ground state.

We outline several reasons why atomic titanium is an attractive choice for ultracold-atom experiments.

A. Anisotropic optical polarizability

The nonzero ($L = 3$) orbital angular momentum of the ground state of Ti indicates that light-atom interactions remain anisotropic even for light that is far-detuned from atomic resonances. We have verified this property by computing the relative strengths $\alpha_S(\omega)$, $\alpha_V(\omega)$, and $\alpha_T(\omega)$ of the scalar, vector, and tensor portions of the ground-state ac Stark shift,
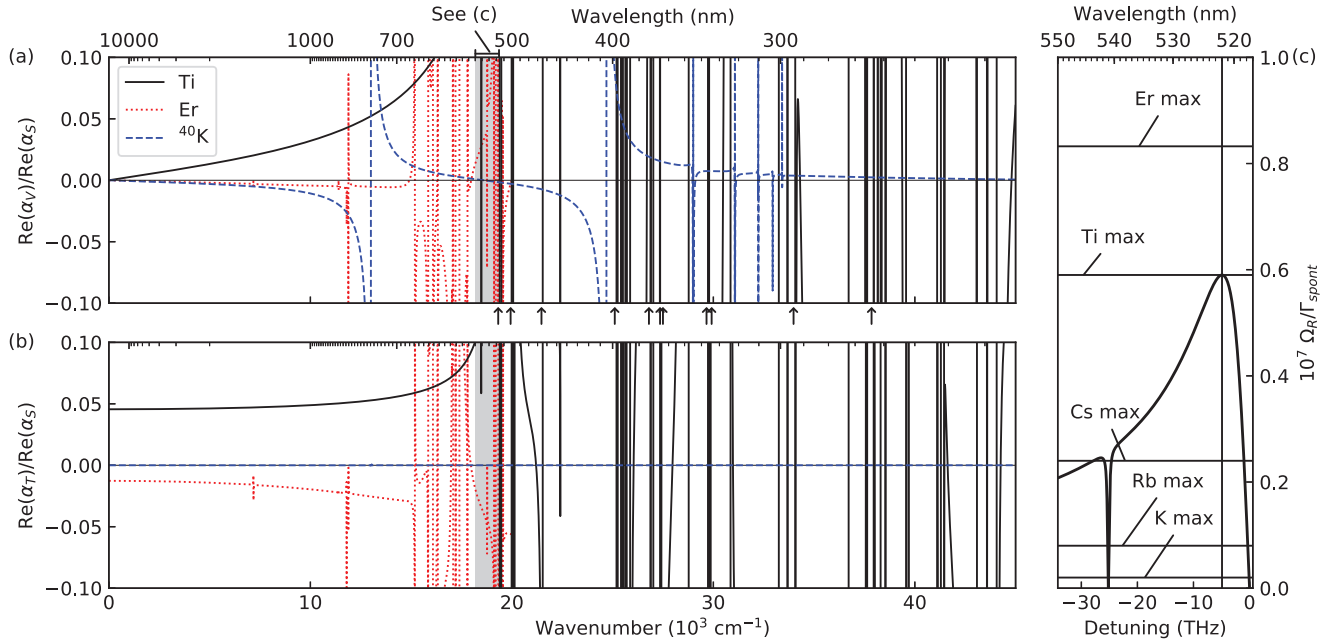
FIG. 1. (a) Vector [Re (α_V)] and (b) tensor polarizability [Re (α_T)] for Ti (solid black), Er (dashed red), and ^{40}K (dotted blue) in their absolute ground states, scaled by the scalar polarizability Re (α_S), and plotted as a function of the wave number and wavelength of applied light. Arrows indicate all transitions to an excited $3d^2 4s4p$ state in Ti with an oscillator strength greater than 0.01. The data for Er, reproduced from Ref. [20], showing the dense spectrum above 20 000 cm^{-1} is omitted for clarity. (c) The figure of merit $\mathcal{M} = \Omega_R / \Gamma_{sp}$ is plotted over the narrow wavelength range indicated by a gray band in (a) and (b), with detuning measured relative to the $a\,^3F_2 \rightarrow z\,^3F_2^\circ$ transition. Solid horizontal lines indicate the maximal $\mathcal{M}$ achievable in the Raman coupling scheme for each element, while the vertical line indicates the corresponding wavelength ($\sim$522 nm) in Ti.

respectively, as a function of the optical frequency ω. Here, we express the total ac Stark shift $\alpha_{m_J}(\omega)$, for an atom in the m_J magnetic sublevel defined with respect to a quantization axis **b**, as [12,29]

$$\alpha_{m_J}(\omega) = \alpha_S(\omega) + (\mathbf{k} \cdot \mathbf{b}) \mathcal{A} \frac{m_J}{2J} \alpha_V(\omega)$$
$$+ \frac{1}{2}\big(3|\boldsymbol{\epsilon} \cdot \mathbf{b}|^2 - 1\big) \frac{3m_J^2 - J(J+1)}{J(2J-1)} \alpha_T(\omega). \quad (1)$$

In this expression, **k** is the unit wave vector and $\mathcal{A}$ the helicity of the light field, and $\boldsymbol{\epsilon}$ is the optical polarization vector.

We calculate the ac Stark shift by taking into account all electric-dipole optical transitions identified in the NIST Spectral Database [30] for neutral titanium, using the reported oscillator strengths for all lines for which such strengths are provided. In addition, there are several excited fine-structure levels for which an oscillator strength is not directly reported, but for which we can estimate such strength based on that reported for a different level of the same configuration and term [31]. As an example, the $a\,^3F_2 \rightarrow w\,^3D_1^\circ$ and $a\,^3F_2 \rightarrow w\,^3D_2^\circ$ transitions have reported line strengths of 0.71 and 0.051 a.u., respectively, while the line strength of the $a\,^3F_2 \rightarrow w\,^3D_3^\circ$ transition is not reported. Using the results for LS coupling, we estimate that the unobserved line strength is approximately 0.02 a.u. Our calculation only accounts for transitions with reported or estimated transition rates, and neglects contributions to the atomic polarizability from both the above-ionization continuum and weaker lines without measured transition rates. Nevertheless, it provides a

reasonable estimate for the nature of the ac Stark shifts for long-wavelength ($\lambda \geqslant 500$ nm) laser light. A similar approach was followed, for example, by Tsyganok *et al.* [32].

The anisotropy of light-atom interactions is characterized by the ratios Re (α_V)/Re (α_S) and Re (α_T)/Re (α_S). Figure 1 shows these calculated ratios for Ti, and compares them to similar ratios calculated for potassium (K) and erbium (Er).

Examining the long-wavelength limit, i.e., far-red-detuned from atomic transitions, we find the polarizability of Ti to be dramatically more anisotropic than for the alkali-metal atom K. We focus specifically on the isotope ^{40}K, which, similar to the fermionic isotopes of Ti, is suited to studies of fermionic quantum matter. In K, two transitions contribute dominantly to the optical response: the D_1 line ($4s\,^2S_{1/2} \rightarrow 4p\,^2P_{1/2}^\circ$) at 770.1-nm wavelength and linewidth $2\pi \times 6.01$ MHz, and the D_2 line ($4s\,^2S_{1/2} \rightarrow 4p\,^2P_{3/2}^\circ$) at 766.7-nm wavelength and linewidth $2\pi \times 5.94$ MHz. Strongly anisotropic polarizability is obtained for light that is tuned near one or the other of these transitions. However, for light that is much farther detuned than the approximately terahertz frequency separation between these fine-structure lines so that the detuning to each of these transitions is nearly the same, the atomic polarizability becomes nearly isotropic. At a pictorial level, we can consider that the electron distribution in the ground state of K, with a single valence electron in an s orbital, is isotropic; hence, it responds isotropically to light of any optical polarization. Coupling between the optical polarization and the electron spin is obtained only by exploiting the spin-orbit coupling (i.e., resolving the fine-structure splitting) of the excited state.

In contrast, Ti and also Er show significantly anisotropic interactions in wide parts of the optical spectrum, including far from atomic resonances. The electronic ground state of Ti is calciumlike, with a strong optical response produced by excitations of the valence $4s^2$ electrons to the $4s4p\,(^1P^\circ)$ excited-state configuration. For Ca, this excitation occurs at a single transition at 432-nm wavelength. In contrast, in Ti this excited-state configuration is split into numerous terms (indicated by arrows in Fig. 1) because of interactions with the partly filled ($L \neq 0$) $3d$ shell, with the optical coupling strength to each term depending on the optical polarization and the angular momentum state of the $a\,^3F_2$ ground-state atom. The excited energy terms are split by large electron-correlation energies, on the order of hundreds of terahertz, leading to large differential detunings for long-wavelength light from each of the relevant excited states. Altogether, the state-dependent coupling and the large energy differences of these many states results in a strongly anisotropic light-atom interaction. A similar argument explains the similarly anisotropic polarizability of Er.

An important figure of merit for cold-atom experiments that make use of anisotropic light-atom interactions is the ratio $\mathcal{M} = \Omega_R/\Gamma_{sp}$ between the coherent and the incoherent parts of the interaction. Here, Ω_R is the Rabi frequency for Raman transitions between different angular momentum states within the electronic ground state, or, equivalently, the vector or tensor ac Stark shift divided by $\hbar$, while Γ_{sp} is the total spontaneous emission rate. Highly coherent (large $\mathcal{M}$) interactions can be achieved for light that is far-red-detuned from all optical transitions. Denoting $\mathcal{M}_{V,T}$ for the vector and tensor coupling figures of merit, respectively, in the far-red-detuned regime, we estimate the average figure of merit as $\mathcal{M}_{V,T} \sim \mathrm{Re}\,(\alpha_{V,T})/|\mathrm{Im}\,(\alpha_S)|$. For example, considering light at a wavelength of 1 μm, as commonly used in optical-lattice experiments, we expect $\mathcal{M}_V \sim 4 \times 10^5$, $\mathcal{M}_T \sim 5 \times 10^6$ for Ti, compared to $\mathcal{M}_V \sim 4 \times 10^3$, $\mathcal{M}_T \sim 1 \times 10^6$ for Er, and $\mathcal{M}_V \sim 1.5 \times 10^5$, $\mathcal{M}_T \sim 1.5$ for ^{40}K.

Alternately, highly coherent light-atom interactions can be found for light at frequencies that are closer to specific atomic resonances. For example, Refs. [33,34] propose the use of narrow-line excitations to achieve anisotropic light-atom interactions in Er. Considering scattering just from the narrow-line resonance itself, the ratio $\mathcal{M}$ generally increases with detuning Δ between the optical and resonance frequencies, with $\Omega_R \propto \Delta^{-1}$ and $\Gamma_{sp} \propto \Delta^{-2}$. However, at large enough Δ, spontaneous emission from all other atomic resonances becomes dominant, establishing an upper limit of $\mathcal{M}$. Near a particular atomic resonance, the figure of merit can be approximated as [33,34]

$$\mathcal{M} \approx \frac{2\Delta_i}{\Gamma_i + \sum_{j \neq i} \Gamma_j \frac{\Delta_i^2}{\Delta_j^2}\frac{A_j}{A_i}}, \quad (2)$$

where Δ_i is the optical detuning from the particular transition chosen, $A_{i,j}$ are Einstein A coefficients that describe the optical excitation strength from the atomic ground state to each excited state, and $\Gamma_{i,j}$ are transition line widths. The summation in the denominator is taken over all optical transitions other than the particular transition leverage for its anisotropic polarizability. For Er, this expression gives a max-

imum of $\mathcal{M} \sim 8 \times 10^6$. A similar approach appears possible in atomic Ti. For example, examining the spectrum of Ti, we find a similar figure of merit, $\mathcal{M} \sim 6 \times 10^6$, for generating state-dependent optical interactions with light that is detuned from the transition between the atomic ground state and the $3d^2(^3F)4s4p(^3P^\circ)z\,^3F_2^\circ$ excited state, with wavelength 518 nm. It is notable that this highly coherent, anisotropic light-atom interaction is achieved with light near the 530-nm-wavelength range that is easily produced at high power by frequency-doubled laser systems.

B. Magnetic dipolar relaxation

While Ti and the lanthanides Er and Dy both allow for highly coherent anisotropic light-atom interactions, Ti, in its $a\,^3F_2$ ground state, has the additional advantage of being relatively stable against inelastic magnetic-dipolar relaxation. The rate of dipolar relaxation induced by the long-range dipole-dipole interaction in ultracold gases, as considered in Refs. [35–37], scales (for the magnetic dipole–magnetic dipole case) as the square of the magnetic moment $\mu = g_J J \mu_B$, with g_J being the Landé g factor, J being the atomic total angular momentum, and μ_B being the Bohr magneton. Magnetic dipolar relaxation in highly magnetic atoms such as Dy [19] and Cr [37], with magnetic moments of $\mu = 10\,\mu_B$ and $6\,\mu_B$, respectively, is rapid, leading to spin-polarization lifetimes on the order of 1 s or below under common experimental gas densities ($\sim 10^{13}$ cm^{-3}) and applied magnetic fields ($\sim$1 G). In contrast, for alkali-metal atoms, with magnetic moments of $1\mu_B$ and below, the minutes-long stability of magnetically trapped atoms indicates the dipolar relaxation rate to be very small.

For Ti, the $J = 2$, 3, and 4 ground states have magnetic moments of $g_J J \mu_B = 4/3\,\mu_B$, $13/4\,\mu_B$, and $5\,\mu_B$, respectively. Since the magnetic moment of the overall ($J = 2$) ground state is similar in magnitude to that of an alkali-metal atom, we expect dipolar relaxation in a $a\,^3F_2$ Ti gas to be very slow. Additional inelastic decay paths could be opened by interactions between the open d shells of the colliding atoms. However, several studies, e.g., theoretical studies on Sc [38,39] and experiments on buffer-gas-cooled Ti gases [40], indicate that such inelastic processes are suppressed by the fact that the $3d$ shell is submerged below the closed $4s$ shell. Altogether, collisions among ground-state Ti atoms should be predominantly spin preserving, allowing, for example, for magnetic trapping in weak-field seeking states and for studies of spinor gases with conserved magnetization.

C. Isotopic richness

Another favorable property of Ti is that it is endowed with numerous stable isotopes, presenting a broad palette of choices for ultracold atomic gas experiments. These choices include three bosonic isotopes, ^{46,48,50}Ti, with relatively large natural abundance (8%, 74%, and 5%, respectively). All three bosonic isotopes have nuclear spin $I = 0$, leading to a simple atomic-level structure that is free of hyperfine structure. As quantum-degenerate gases, these three isotopes, in their $a\,^3F_2$ ground state, may present examples of $J = 2$ spinor Bose-Einstein condensates, which are predicted to manifest three

different types of magnetic ordering: ferromagnetic, nematic, and tetragonal [41–43]. The choice of ground state depends on the relative strengths of three s-wave scattering lengths that characterize the low-energy collisions between $J = 2$ bosons. Both the nematic and tetragonal phases, owing to their discrete rotational symmetries, support structures such as fractional superfluid vortices [44–46], whose non-Abelian character can lead to complex vortex collision and rung dynamics [47]. While ^{87}Rb does already permit studies of $F = 2$ spinor gases in its higher-energy hyperfine spin manifold, such gases have only limited lifetimes (of order 100 ms at typical densities) owing to hyperfine relaxation collisions.

Ti also has two stable fermionic isotopes, ^{47,49}Ti, with nuclear spins $I = 5/2$ and $7/2$, and abundances of 7% and 5%, respectively. Given the strong anisotropy of light-atom interactions, and the stability of spin mixtures against dipolar relaxation, these isotopes could be used to study Cooper pairing in spin-orbit coupled Fermi gases. Such systems, which are under investigation also within solid-state devices, are predicted to support topological superfluidity and Majorana fermions [48–50], with relevance to topological quantum computing [51–53].

D. Laser-cooling scheme

Many successful realizations of laser cooling make use of atomic transitions that are approximately closed, driving an atom from a low-energy state of angular momentum J to an excited state of angular momentum $J + 1$. The closed nature of the transition ensures than an atom will scatter the large number of photons (10^3 or greater) required to reduce its velocity through the optical scattering force, returning always to the laser-cooling state. The $J \rightarrow J + 1$ nature of the transition provides for optical pumping of the atom into a brightly scattering state and enables techniques such as magneto-optical trapping and polarization-gradient cooling.

There is no $J \rightarrow J + 1$ transition from the $a\,^3F$ ground term of titanium that satisfies these criteria. The optical spectrum of this ground term, dominated by excitation of one of the $4s^2$ electrons of the ground configuration, resembles that of calcium. As in the case of calcium [54–56], laser cooling via one of these transitions is unfavorable since there is significant leakage from the excited states to other even-parity metastable states.

Instead, a suitable laser-cooling transition is found among the family of lines that arise after exciting an electron to a metastable alkali-metal-like configuration $3d^3 4s^1$. The lowest energy level of this metastable configuration, the $a\,^5F$ level, is split via fine structure into $J = 1$ to $J = 5$ states. While the lifetime of these states has not been measured, the two dominant decay mechanics, magnetic dipole radiation between fine-structure states and spin-forbidden electric quadrupole decay to the ground state, are weak transitions. Comparing to similar atoms, such as Fe, we expect the radiative lifetime of these states to be on the order of 10–100 s [30]. The highest-J state, labeled $a\,^5F_5$ and with an energy of 6843 cm^{-1} above the ground state, has a strong $J \rightarrow J + 1$ transition to the odd-parity $y\,^5G_6^\circ$ state (at energy 26 911 cm^{-1}). On this transition, at a wavelength of 498.3 nm, the valence $4s_{1/2}$ electron is excited to the $4p_{3/2}$ level. The remaining valence

electrons remain in the spin-polarized $3d^3(^4F_{9/2})$ configuration. As such, the transition resembles the D_2 $4s \rightarrow 4p$ transition in potassium if we regard Ti's $3d^3$ valence electrons as part of the inert atomic core. The linewidth of this transition ($\Gamma = 2\pi \times 10.5$ MHz) is comparable to that of alkali-metal atom cooling transitions, with a corresponding Doppler cooling limit of $T_D = \hbar\Gamma/(2k_B) = 250$ μK. This line is amenable to all the standard tricks of laser-cooling: Zeeman slowing, magneto-optical trapping, and polarization-gradient cooling. Furthermore, the line is sufficiently broad to provide a strong cooling force.

This transition appears to be a cycling transition because of the spin-polarized nature of the $3d^3$ electrons and the maximal $J = 5$ value of the total electronic angular momentum. Electric-dipole transitions could, in principle, lead from the odd-parity excited state to four other even-parity states: the $a\,^3G_5$ state (at energy of 15 220 cm^{-1}), the $a\,^3H_{5,6}$ states (18 141 cm^{-1} and 18 192 cm^{-1}, respectively), and the $a\,^1H_5$ state (20 796 cm^{-1}). However, these transitions are all spin forbidden, requiring a reconfiguration of the $3d^3$ valence electrons. Focusing on the leakage into states with $J = 5$, we estimate the residual branching ratio for spontaneous emission into these states by considering the degree to which a spin-orbit interaction term would mix these states with the $a\,^5F_5$ state. We quantify the strength of the spin-orbit mixing energy from the fine-structure splitting of the $a\,^5F_5$ level, and then apply second-order perturbation theory to estimate the branching ratio as $P_i = \delta^2/\Delta_i^2$, where $\delta = E_{a\,^5F_5} - E_{a\,^5F_4}$ is the fine-structure splitting and $\Delta_i = E_i - E_{a\,^5F_5}$ is the difference in energy between a given leakage state i and the $a\,^5F_5$ state. Under these assumptions, we expect that the total leakage $P = \sum_i P_i = \sum_i \frac{\delta^2}{\Delta_i^2}$ from the cooling transition to be around 3×10^{-5}, low enough to perform laser cooling and trapping without the need for constant repumping lasers. For the remaining atoms being considered, the leakage is also small and not reported in any spectroscopic data. We calculated the leakage through this same method of estimating the mixing between states of different spins by the ratio δ/Δ_i for the given possible leakage states.

The $a\,^5F_5$ state supports an additional cycling transition. This transition to the $z\,^5G_6^\circ$ state has an optical wavelength of 1040 nm and a linewidth of $2\pi \times 11.3$ kHz, giving a Doppler temperature of $T_D = 0.27$ μK. As has been demonstrated with Sr [57,58], Ca [59], Yb [60], Dy [15], and Er [61], a second-stage magneto-optical trap (MOT) using this narrower line could significantly increase the phase-space density of the laser-cooled gas. Furthermore, there are even fewer leakage channels for emission out of the $z\,^5G_6^\circ$ state than out of the $y\,^5G_6^\circ$ state, increasing the number of photons that could be scattered without the need for repumping. By the same method of estimation, we expect the leakage from this transition to be around 1×10^{-7}.

Producing an atomic beam of Ti through direct sublimation requires a Ti source to be heated to temperatures upwards of 1500 K. At this high temperature, almost 0.1% of the sublimated atoms will be thermally excited into the metastable laser-cooling state. A higher population in the laser-cooling state can be achieved by optical pumping of ground-level atoms. To find a promising excited state e for efficient optical
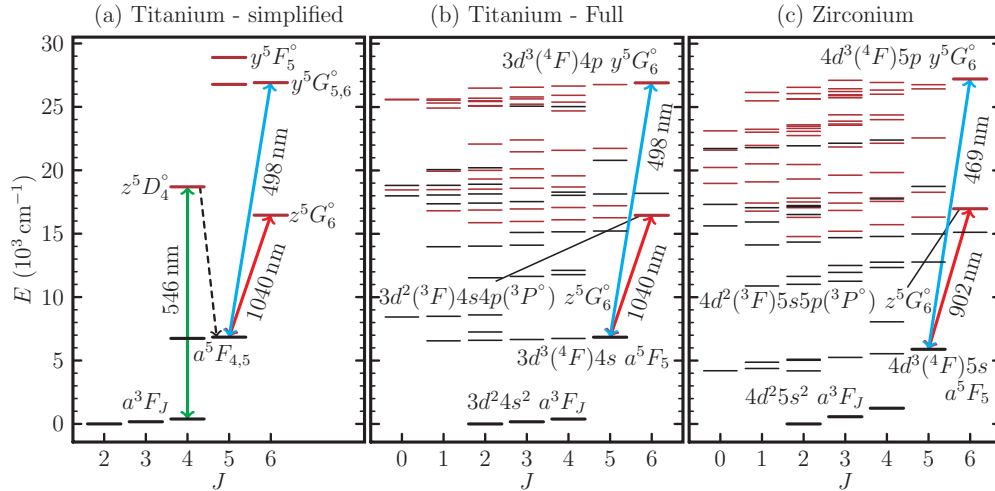
FIG. 2. Energy levels of titanium group elements Ti and Zr. Here, and in subsequent energy-level figures, black (red) lines indicate even- (odd-) parity states, and thicker lines highlight states relevant for laser cooling. Levels are arranged by total electronic angular momentum J and ordered by energy. (a) Shows a simplified energy-level diagram of Ti, highlighting the important levels and transitions involved in the entire laser-cooling scheme. The $a\,^3F_J$ fine-structure ground levels and $a\,^5F_5$ metastable laser-cooling level are the relevant even-parity states. The $z\,^5D_4^\circ$ level is one of several intermediate states that could be used to optically pump atoms into the $a\,^5F_5$ state, with the 546-nm transition indicated as well as the dominant decay path. The two excited levels for laser cooling, the $z\,^5G_6^\circ$ and $y\,^5G_6^\circ$, are also identified and can support type-I MOTs with transitions at 1040 nm (red) and 498 nm (blue), respectively. (b) A more complete diagram of Ti levels is given, including the full configuration and term symbol for the ground states and laser-cooling excited states. For simplicity, optical pumping transitions are suppressed. All levels below the $y\,^5G_6^\circ$ state are shown. (c) Zr-level structure. All levels below the $y\,^5G_6^\circ$ are shown. The laser-cooling transitions, analogous to those in Ti, are shown as well.

pumping from a ground state g to a target state t, we have examined the available data on the NIST database. Under the assumptions that we have sufficient laser power to drive the optical pumping transition and that the leakage out of the optical pumping transition to other metastable dark states d_i is sufficiently captured by existing data, we calculate the efficiency of an optical pumping transition as

$$\eta = \frac{A_{eg} + A_{et}}{A_{eg} + A_{et} + \sum_i A_{ed_i}} = \frac{A_{eg} + A_{et}}{\Gamma_e}. \quad (3)$$

In titanium, we identify three promising schemes for transferring atoms from the $a\,^3F_4$ state into the $a\,^5F_5$ state: one-color optical pumping via the $z\,^5D_4^\circ$ state (wavelength $\lambda = 546.20$ nm, linewidth $\Gamma = 2\pi \times 0.3$ MHz, transfer efficiency $\eta = 0.88$), one-color optical pumping via the $y\,^5F_5^\circ$ state ($\lambda = 350.76$ nm, $\Gamma = 2\pi \times 16$ MHz, $\eta = 0.9$), or two-color pumping via the $y\,^5G_5^\circ$ state ($\lambda = 378.99$ nm, $\Gamma = 2\pi \times 12.7$ MHz), and $y\,^5F_5^\circ$ state ($\lambda = 451.40$ nm, $\Gamma = 2\pi \times 15.7$ MHz). In the two-color scheme, the first transition pumps the majority of the atoms into the $a\,^5F_4$ state, which is then pumped by the second transition to the laser-coolable $a\,^5F_5$ state, for a total efficiency of $\eta = 0.995$. There are multiple routes to transfer atoms from the $a\,^5F_5$ state to the $a\,^3F_2$ ground state; one simple path would be to drive the $a\,^5F_5 \rightarrow z\,^3F_4^\circ$ transition at 758 nm, which transfers atoms to the $a\,^3F_4$ and $a\,^3F_3$ states. Simultaneously driving the $a\,^3F_4 \rightarrow y\,^3F_3^\circ$ and $a\,^3F_3 \rightarrow y\,^3F_2^\circ$ transitions at the wavelengths of 403 and 401 nm leads to a total transfer efficiency of $\eta = 0.814$ for transferring $a\,^5F_5$ atoms to the $a\,^3F_2$ ground state. More efficient schemes come at the cost of greater experimental complexity.

III. TITANIUM AND IRON GROUP ATOMS

A. Titanium group

Other elements in the titanium group, zirconium (Zr) and hafnium (Hf), have similar atomic structures and spectra to Ti. There are two low-energy, even-parity electronic configurations, in which the four valence electrons reside in either an alkaline-earth-metal-like configuration of $(n-1)d^2 ns^2$ or an alkali-metal-like configuration $(n-1)d^3 ns^1$ where n is the principal quantum number of the valence s shell. The ground level has the configuration $(n-1)d^2 ns^2$ and term symbol $a\,^3F_2$, with fine-structure splitting to other J levels on the order of 100 cm^{-1}. The lowest-energy state with the $(n-1)d^3 ns^1$ electron configuration has a term symbol $a\,^5F$ and the spin-polarized laser-cooling state is identified as the highest fine-structure state with $J = 5$.

1. Zirconium

The level structure of Zr is shown in Fig. 2. The laser-cooling state lies 5889 cm^{-1} above the ground state. A strong laser-cooling transition to the $y\,^5G_6^\circ$ state lies at a wavelength of 468.9 nm. An additional closed cooling transition, to the $z\,^5G_6^\circ$ state, occurs at the wavelength 901.8 nm. Linewidths for these two transitions have not been measured. However, one expects linewidths similar to those found in Ti, i.e., that the blue-light transition, which involves an $(n-1)d^3 ns \rightarrow (n-1)d^3 np$ electron configuration change, will have a linewidth in the range of $2\pi \times 10$ MHz, while the red transition, which involves an $(n-1)d^3 ns \rightarrow (n-1)d^2 ns\,np$ core-electron configuration change, will be substantially narrower than the blue-light transition. Given the increased
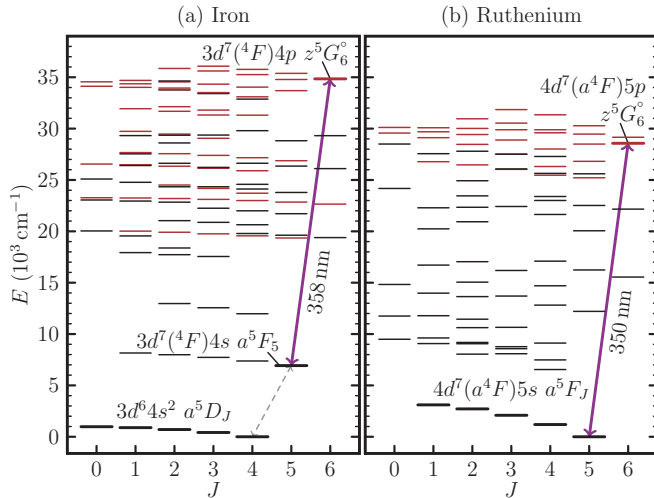
FIG. 3. Energy levels of iron group elements (a) Fe and (b) Ru. In Fe, the metastable laser-cooling state is the $a\,^5F_5$ state. The laser-cooling transition at 358-nm wavelength drives the atom to the $z\,^5G_6^\circ$ excited state. Laser cooling on this transition has been demonstrated [28,62]. Indicated by the dashed gray arrow is the decay of the $a\,^5F_5$ state in Fe, predicted to occur at a rate of 2×10^{-3} s^{-1} [30]. In Ru, the $a\,^5F_5$ laser-cooling state is also the overall ground state, eliminating the need for optical pumping into a metastable state. The 350-nm wavelength laser-cooling transition, connected to the $z\,^5G_6^\circ$ state is indicated.

spin-orbit coupling of Zr, leakages from the excited states are expected be greater than in Ti. We expect the leakage for the broad (narrow) transition to be around 1×10^{-4} (1×10^{-5}). Zr possesses six stable or long-lived naturally abundant isotopes: four bosonic isotopes (^{90,92,94,96}Zr) with nuclear spin $I = 0$, and two fermionic isotopes (^{91,93}Zr) with $I = 5/2$.

2. Hafnium

The spectrum of Hf is too poorly known to determine whether the analogous laser-cooling transition exists below the first ionization limit (55 047.9 cm^{-1}). However, there is a metastable state that should be long-lived and might support laser cooling: the $5d^3(b\,^4F)6s\,a\,^5F_5$ state with an energy of 17 901.28 cm^{-1} above the ground state.

B. Iron group

The elements in the iron group, iron (Fe), ruthenium (Ru), and osmium (Os), also have two low-energy even-parity electronic configurations: an alkaline-earth-metal-like valence configuration $(n-1)d^6\,ns^2$ and the alkali-metal-like valence configuration $(n-1)d^7\,ns^1$ (Fig. 3). As in the titanium group, a cycling transition exists on the maximum-J level of the lowest-energy alkali-metal-like level, also given by the term symbol $a\,^5F_5$. However, because the valence d orbital of the iron group is more than half filled, metastable states do not enjoy the protection from decay afforded by a required spin flip; the total spin S of the ground and metastable cooling states are equal.

1. Iron

Laser cooling of iron (Fe) has been realized by the Bastin group [62]. The ground level of Fe has an electron configuration of $3d^6\,4s^2$ and term symbol $a\,^5D_J$, with total angular momenta J ranging from $J = 0$ to $J = 4$. The overall ground state, $a\,^5D_4$, has a large magnetic moment and is expected to undergo significant magnetic dipole-dipole relaxation. The metastable cooling state $3d^7(^4F)\,4s\,a\,^5F_5$, with an energy of 6928 cm^{-1}, has an estimated lifetime between 300 and 1000 s [30], allowing ample time for cooling and trapping of Fe atoms. This state has a closed transition to the excited state $3d^7(^4F)\,4p\,z\,^5G_6^\circ$ with a wavelength of 358 nm and a linewidth of $2\pi \times 16.2$ MHz. Similar to Ti, it is possible in Fe to increase the population of atoms in the metastable cooling state via optical pumping; in Ref. [28], the 372-nm-wavelength transition to the $z\,^5F_5^\circ$ state is used. While not reported in the literature, we expect the leakage from the cooling transition to be around 4×10^{-5}.

2. Ruthenium

Ruthenium (Ru) may be a surprisingly convenient choice for laser cooling. For this atom, the laser-cooling state $a\,^5F_5$ is indeed the overall ground state, obviating the need for optical pumping to drive atoms into the laser-cooling state. Laser cooling would proceed directly through the transition to the $z\,^5G_6^\circ$ excited state at a wavelength of 350 nm and with a linewidth of $2\pi \times 13.7$ MHz. The leakage from this transition is expected to be around 7×10^{-4}.

Ru has several additional features of interest. First, the spectrum of Ru should contain a narrow-line magnetic dipole transition from the metastable even-parity $4d^7(a\,^4F)\,5s\,a\,^5F_1$ state up to the low-lying $4d^6 5s^2\,a\,^5D_0$ excited state. This transition frequency should be insensitive at first order to applied magnetic fields. Moreover, light at the transition wavelength of 1566 nm could be transmitted at low loss through optical fibers. The excited state, which can decay either on a magnetic dipole transition towards the $a\,^5F_1$ state, on an electric quadrupole transition to the $a\,^5F_2$ state, or on a two-photon electric dipole transition to the $a\,^5F_1$ state, should be very long-lived. Altogether, this transition could offer advantages as an optical clock standard. Second, Ru has a large number of stable isotopes, including five bosonic isotopes (^{96,98,100,102,104}Ru) with a nuclear spin $I = 0$. The isotope shifts on the various narrow-line transitions in Ru could be leveraged to search for forces outside the standard model [63].

3. Osmium

As with Hf, the spectrum of Os is not known well enough to determine whether there is a closed laser-cooling transition below the first ionization limit. However, the $5d^7(^4F)\,6s\,a\,^5F_5$ metastable state (energy of 5144 cm^{-1}) would likely have a long lifetime and could support laser cooling

IV. SCANDIUM, VANADIUM, AND MANGANESE GROUP ATOMS

The general method of cooling gases of transition metals proposed herein—employing a long-lived alkali-metal-like metastable state with configuration $(n-1)d^{x+1}\,ns^1$ consisting
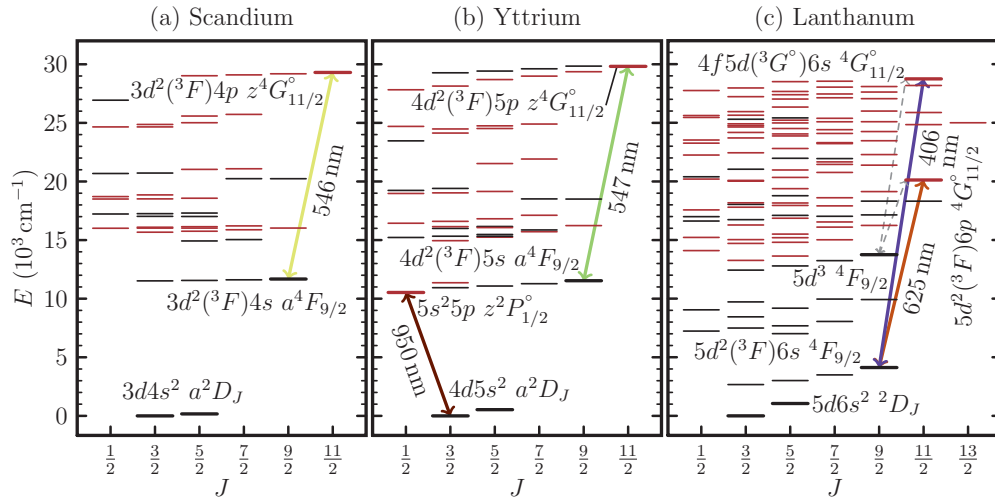
FIG. 4. Energy levels of scandium group elements (a) Sc, (b) Y, and (c) La. The $a\,^2D_J$ ground term and $a\,^4F_{9/2}$ metastable laser-cooling state are highlighted in all diagrams. For Sc, the laser-cooling transition at 549-nm wavelength connects to the $z\,^4G_{11/2}$ state. In Y, the analogous transition occurs at wavelength 547 nm; also indicated is the narrow laser-cooling transition for the ground state at wavelength 950 nm. For La, two laser-cooling states at wavelengths 625 and 406 nm connect to two $^4G_{11/2}$ states. The gray dashed arrows indicated two potential spin-allowed leakage paths that may require repumping.

of a polarized submerged shell core and a single valence s electron—is applicable also to several other transition-metal atoms. Table I gives the relevant properties for the metals of the scandium, vanadium, and manganese group that we have identified as amenable to laser cooling. We discuss these cases briefly below.

A. Scandium group

Atoms in the scandium group—Sc, Y, and La—have a ground state characterized by two valence s electrons [$(n-1)d^1\,ns^2\,a\,^2D_{3/2}$], where n is the principal quantum number of the valence shell (with n being 4, 5, or 6 for Sc, Y, and La, respectively) and a spin-polarized metastable alkali-metal-like configuration [$(n-1)d^2\,ns^1\,a\,^4F_J$]. The laser-cooling state is given by the highest fine-structure level $J = 9/2$ of this metastable state from which a strong, closed $J + 1$ transition exists up to an odd-parity excited state $z\,^4G_{11/2}^\circ$ (see Fig. 4 for atomic-level structures).

1. Scandium

In scandium (Sc), the cooling scheme proceeds without any mitigating factors. The laser-cooling transition occurs at 567.3402 nm [64] with a linewidth of $2\pi \times 8.6$ MHz [65]. Sc possesses one stable isotope, bosonic ^{45}Sc, with nuclear spin $I = 7/2$.

2. Yttrium

In Y, there is the laser-cooling line from a metastable state as described above, with a wavelength of 546.7986 nm [66] and a linewidth of $2\pi \times 10$ MHz [67]. Yttrium possesses one stable isotope, bosonic ^{89}Y, with nuclear spin $I = 1/2$.

A second transition may also be considered, between the overall ground state $4d5s^2\,a\,^2D_{3/2}$ and the lowest odd-parity excited state, $5s^25p\,z\,^2P_{1/2}^\circ$. As a $J \to J - 1$ transition, this excitation would be suited to a type-II magneto-optical trap

[68]. While the transition itself has not yet been observed, its wavelength of 949.7429 nm is known [69]. There are no possible leakage channels for this transition, allowing a clear cycling transition to be used. It would likely be a relatively narrow E_1 transition, since it involves the transition of the inner shell $4d$ electron to the $5p$ state.

3. Lanthanum

Lanthanum (La) returns to the pattern of only being coolable from a metastable state. However, it has two possible cycling transitions available in this state. One laser-cooling transition connects the metastable $5d^2(^3F)6s\,^4F_{9/2}$ and the $5d^2(^3F)6p\,^4G_{11/2}^\circ$ state, occurring at 625.166 nm [66] with a linewidth of $2\pi \times 5.86$ MHz [70]. A second transition connects the metastable state to the excited state $4f5d(^3G^\circ)6s$ $^4G_{11/2}^\circ$, with wavelength 406.148 nm [66] and linewidth $2\pi \times 8.9$ MHz [70]. Lanthanum possesses one stable isotope, bosonic ^{139}La, with a nuclear spin $I = 7/2$. However, fermionic ^{138}La is long-lived, with a half-life of 1.02×10^{11} yr, which could allow an isotopically enriched sample of fermionic atoms to be studied. ^{138}La has a nuclear spin $I = 5$.

Lanthanum also has a difficulty not present in the other elements that have been discussed: from both of the excited states that could be addressed for laser cooling, there is a spin-allowed electric-dipole transition to the $5d^3\,^4F_{9/2}$ state. While decay to this state has not been observed, it could be a stronger source of leakage than in the other examples considered thus far. If these leakage channels are significant, they could be repumped to replenish the atoms in the metastable cooling state.

B. Vanadium group

In both vanadium (V) and niobium (Nb), the alkali-metal-like, even-parity state with stretched J, the $(n-1)d^4(^3H)ns^1$ $a\,^4H_{13/2}$ state, is viable for laser cooling (Fig. 5). In both
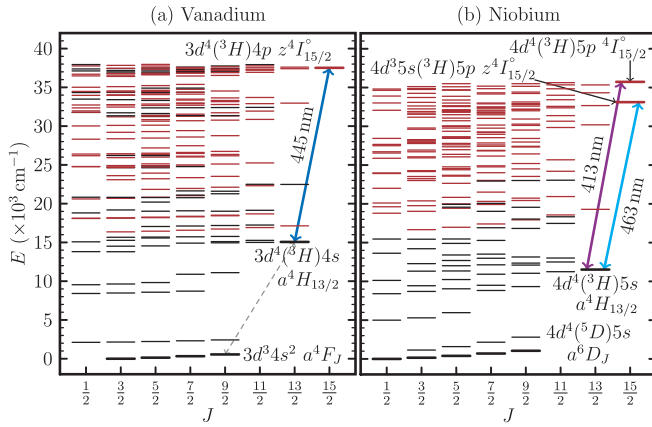
FIG. 5. Energy levels of vanadium group elements (a) V and (b) Nb. The fine-structure ground states (a^4F for V, a^6D for Nb), metastable laser-cooling state a $^4H_{13/2}$, and z $^4I_{15/2}^{\circ}$ state are indicated. The laser-cooling transitions (wavelengths 445 nm for V, 463 nm for Nb) are also indicated. In dashed gray is indicated the dominant decay path of the metastable state of Nb atoms, an E_2 transition with $A_{ki} \sim 2\pi \times 130$ mHz [30].
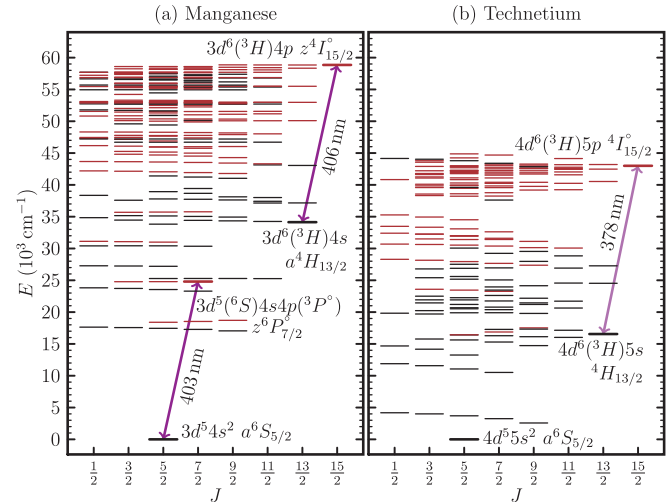

FIG. 6. Energy levels of manganese group elements (a) Mn and (b) Tc. Both Mn and Tc possess a viable cycling transition (wavelengths 406 and 378 nm) between the metastable a $^4H_{13/2}$ state and the z $^4I_{15/2}^{\circ}$ state. Mn is also likely laser coolable directly in the ground state. The three possible laser-cooling transitions are at a wavelength of 403 nm and connect the a $^6S_{5/2}$ ground state to the z $^6P_J^{\circ}$ states.

atoms, it connects to cycling transitions with the $(n-1)d^4(^3H)\,np^1\,z\,^4I_{15/2}^{\circ}$, while Nb possesses an additional cooling transition.

1. Vanadium

For V, the laser-cooling transition occurs at wavelength 445 nm with a linewidth of $\Gamma = 2\pi \times 13$ MHz. There is only one other $J = 13/2$ even-parity state where leakage from this cycling transition could occur; we estimate the leakage to be 2×10^{-6}. The radiative lifetime of the a $^4H_{13/2}$ state has been calculated to be ~ 1.2 s [30], occurring via electric quadrupole decay to the a $^4F_{9/2}$ state.

2. Niobium

For Nb, two laser-cooling transitions exist from the comparable metastable state: the laser-cooling transition comparable to the V transition occurs at wavelength 463 nm between the $a^4F_{13/2}$ and $z^4I_{15/2}^{\circ}$ states. However, there is an additional transition at 413 nm between the metastable state and the $4d^4(^3H)5p$ $^4I_{15/2}^{\circ}$ state. Neither linewidth is known. However, there are no other $J = 13/2$, even-parity states in Nb available for leakage. Thus, we expect the cycling transition, once observed, will be fully closed with respect to electric-dipole decays. However, unobserved even-parity states could in principle introduce leakage channels not listed in atomic structure databases [30]. In this case, the electric-quadrupole decay would be the dominant single-particle loss mechanism for trapped atoms.

C. Manganese group

Elements of the manganese group, manganese (Mn) and technetium (Tc), have ground-state electronic configurations $(n-1)d^5\,ns^2$ and term a $^6S_{5/2}$ (Fig. 6). The stretched J, alkali-metal-like metastable state potentially suitable for laser cooling is the $(n-1)d^6\,ns$ a $^4H_{13/2}$ state.

1. Manganese

The laser-cooling transition of the metastable state in Mn occurs at a wavelength of 406 nm. Its linewidth has not been measured. We expect this transition to be nearly closed, with an estimated leakage of 2×10^{-5}. Mn presents a unique challenge for optical pumping due the high energy of the metastable a $^4H_{13/2}$ state with respect to the $3d^5 4s^2$ a $^6S_{5/2}$ ground state (34 139 cm^{-1}).

However, this ground state may be interesting in its own right, as it possesses several nearly closed electronic transitions with wavelengths near 403 nm that connect to the $3d^5(^6S)\,4s\,4p(^3P^{\circ})\,z^6P_J^{\circ}$ states. While these states likely have spin-allowed leakage channels, the low frequency of these leakage transitions, and the fact that these leakages involve inner electron transitions, may imply that the branching ratio for leakage is very low.

2. Technetium

Unlike in Mn, there is not a closed transition in the ground state of Tc. Indeed, for Tc, contrarily to Mn, the ground state and lowest excited states are much higher in energy relative to the other even-parity metastable states that an atom could leak into. Thus, if one attempted to cycle many photons in the ground state of Tc, it would rapidly leak into a large number of metastable states and be rapidly lost from the trap. However, the metastable cooling state $[4d^6(^3H)5s$ $^4H_{13/2}]$ is of much lower energy (16 553 cm^{-1}) than in Mn, and, thus, is likely easier to access. The laser-cooling transition from this state connects to the $4d^6(^3H)\,5p$ $^4I_{15/2}^{\circ}$ state and occurs at the wavelength 378 nm. Its linewidth has not been reported. Tc is a radioactive element that is not naturally occurring. However, it does have several long-lived isotopes, including bosonic ^{97}Tc and fermionic ^{98}Tc, with half-lives over 10^6 years, and

also the bosonic ^{99}Tc—commonly used in medicine—with a half-life of more than 10^5 years.

V. CONCLUSION

By examining the structure of ground and metastable states of transition-metal atoms, we have identified a number of optical transitions that resemble the principal atomic transitions of alkali-metal atoms, in that a single *s*-orbital valence electron is excited to the *p* orbital at the same principal quantum number. Thus, these transition-metal optical transitions appear suited for laser cooling, i.e., they have large oscillator strength, are nearly cycling with little leakage to additional states, and have the right $J \to J + 1$ angular momentum structure to support many standard laser-cooling techniques. We focus most of our attention on the example of atomic titanium, given that the level structure for this atom is well characterized, that the atom has numerous abundant bosonic and fermionic isotopes, and that its ground state presents attractive features for ultracold atomic physics experiments. The example set by titanium allows us to sift through the level structures of ten other transition-metal elements, and to identify laser-cooling transitions for each.

There remain many potential pitfalls in applying laser cooling to these atomic elements. One possibility is the loss of atoms due to photoionization by laser cooling light. For five of the elements identified (La, V, Nb, Mn, Tc) the excited state in the laser-cooling path is high enough in energy that an additional laser-cooling photon can drive the atom over the first ionization limit. While a calculation of photoionization rates of excited states of atoms is beyond the scope of this paper, such photoionization could present a mechanism to limit the lifetime of atoms in the MOT in addition to the leakage out of the laser-cooling transition and the decay of the metastable state.

Another potential pitfall is that the atoms in metastable states may be subject to strong collisional decay, including light-induced decay in the presence of laser-cooling and optical-pumping light. Even if laser cooling is successful, further cooling toward quantum degeneracy may require multistep optical pumping to the electronic ground state. For some elements, inelastic decay channels in the ground state may be unexpectedly high. Nevertheless, with such a large selection of elements (11) and of stable (26 total) and long-lived (9 total with $> 10^6$ yr half-life) isotopes potentially made available for ultracold atomic physics experiments, the investment of efforts to realize laser cooling of these elements is warranted.

[1] M. Anderson, J. Ensher, M. Matthews, C. Wieman, and E. Cornell, Observation of Bose-Einstein condensation in a dilute atomic vapor, Science **269**, 198 (1995).

[2] K. B. Davis, M.-O. Mewes, M. R. Andrews, N. J. van Druten, D. S. Durfee, D. M. Kurn, and W. Ketterle, Bose-Einstein condensation in a Gas of Sodium Atoms, Phys. Rev. Lett. **75**, 3969 (1995).

[3] J. Stenger, S. Inouye, D. Stamper-Kurn, H.-J. Miesner, A. Chikkatur, and W. Ketterle, Spin domains in ground state spinor Bose-Einstein condensates, Nature (London) **396**, 345 (1998).

[4] M.-S. Chang, Q. Qin, W. Zhang, L. You, and M. Chapman, Coherent spinor dynamics in a spin-1 Bose condensate, Nat. Phys. **1**, 111 (2005).

[5] H. Schmaljohann, M. Erhard, J. Kronjäger, M. Kottke, S. van Staa, L. Cacciapuoti, J. J. Arlt, K. Bongs, and K. Sengstock, Dynamics of $F = 2$ Spinor Bose-Einstein Condensates, Phys. Rev. Lett. **92**, 040402 (2004).

[6] T. Kraemer, M. Mark, P. Waldburger, J. G. Danzl, C. Chin, B. Engeser, A. D. Lange, K. Pilch, A. Jaakkola, H. C. Nägerl, and R. Grimm, Evidence for Efimov quantum states in an ultracold gas of caesium atoms, Nature (London) **440**, 315 (2006).

[7] J. Kinast, S. L. Hemmer, M. E. Gehm, A. Turlapov, and J. E. Thomas, Evidence for Superfluidity in a Resonantly Interacting Fermi Gas, Phys. Rev. Lett. **92**, 150402 (2004).

[8] C. A. Regal, M. Greiner, and D. S. Jin, Observation of Resonance Condensation of Fermionic Atom Pairs, Phys. Rev. Lett. **92**, 040403 (2004).

[9] M. W. Zwierlein, C. A. Stan, C. H. Schunck, S. M. F. Raupach, A. J. Kerman, and W. Ketterle, Condensation of Pairs of Fermionic Atoms near a Feshbach Resonance, Phys. Rev. Lett. **92**, 120403 (2004).

[10] M. Bartenstein, A. Altmeyer, S. Riedl, S. Jochim, C. Chin, J. H. Denschlag, and R. Grimm, Crossover from a Molecular Bose-Einstein Condensate to a Degenerate Fermi Gas, Phys. Rev. Lett. **92**, 120401 (2004).

[11] A. Robert, O. Sirjean, A. Browaeys, J. Poupard, S. Nowak, D. Boiron, C. I. Westbrook, and A. Aspect, A Bose-Einstein condensate of metastable atoms, Science **292**, 461 (2001).

[12] A. Derevianko and H. Katori, *Colloquium*: Physics of optical lattice clocks, Rev. Mod. Phys. **83**, 331 (2011).

[13] A. D. Ludlow, M. M. Boyd, J. Ye, E. Peik, and P. O. Schmidt, Optical atomic clocks, Rev. Mod. Phys. **87**, 637 (2015).

[14] T. Lahaye, T. Koch, B. Frohlich, M. Fattori, J. Metz, A. Griesmaier, S. Giovanazzi, and T. Pfau, Strong dipolar effects in a quantum ferrofluid, Nature (London) **448**, 672 (2007).

[15] M. Lu, N. Q. Burdick, S. H. Youn, and B. L. Lev, Strongly Dipolar Bose-Einstein Condensate of Dysprosium, Phys. Rev. Lett. **107**, 190401 (2011).

[16] K. Aikawa, A. Frisch, M. Mark, S. Baier, A. Rietzler, R. Grimm, and F. Ferlaino, Bose-Einstein Condensation of Erbium, Phys. Rev. Lett. **108**, 210401 (2012).

[17] D. M. Stamper-Kurn and M. Ueda, Spinor Bose gases: Symmetries, magnetism, and quantum dynamics, Rev. Mod. Phys. **85**, 1191 (2013).

[18] N. Q. Burdick, Y. Tang, and B. L. Lev, Long-Lived Spin-Orbit-Coupled Degenerate Dipolar Fermi Gas, Phys. Rev. X **6**, 031022 (2016).

[19] N. Q. Burdick, K. Baumann, Y. Tang, M. Lu, and B. L. Lev, Fermionic Suppression of Dipolar Relaxation, Phys. Rev. Lett. **114**, 023201 (2015).

[20] M. Lepers, J. F. Wyart, and O. Dulieu, Anisotropic optical trapping of ultracold erbium atoms, Phys. Rev. A **89**, 022505 (2014).

[21] W. D. Phillips and H. Metcalf, Laser Deceleration of an Atomic Beam, Phys. Rev. Lett. **48**, 596 (1982).

[22] E. L. Raab, M. Prentiss, A. Cable, S. Chu, and D. E. Pritchard, Trapping of Neutral Sodium with Radiation Pressure, Phys. Rev. Lett. **59**, 2631 (1987).

[23] J. Dalibard and C. Cohen-Tannoudji, Laser cooling below the Doppler limit by polarization gradients: Simple theoretical models, J. Opt. Sci. Am. B **6**, 2023 (1989).

[24] P. Lett, W. Phillips, S. Rolston, C. Tanner, R. Watts, and C. Westbrook, Optical molasses, J. Opt. Sci. Am. B **6**, 2084 (1989).

[25] M. W. Lu, S. H. Youn, and B. L. Lev, Trapping Ultracold Dysprosium: A Highly Magnetic Gas for Dipolar Physics, Phys. Rev. Lett. **104**, 063001 (2010).

[26] J. J. McClelland and J. L. Hanssen, Laser Cooling without Repumping: A Magneto-Optical Trap for Erbium Atoms, Phys. Rev. Lett. **96**, 143005 (2006).

[27] J. Miao, J. Hostetter, G. Stratis, and M. Saffman, Magneto-optical trapping of holmium atoms, Phys. Rev. A **89**, 041401(R) (2014).

[28] J. Crauwels, N. Huet, S. Krins, and T. Bastin, Magneto-optical trapping of iron atoms, Belgian Phys. Soc. Mag. **1**, 17 (2016).

[29] N. L. Manakov, V. D. Ovsiannikov, and L. P. Rapoport, Atoms in a laser field, Phys. Rep. **141**, 320 (1986).

[30] A. Kramida, Y. Ralchenko, J. Reader, and NIST ASD Team, NIST Atomic Spectra Database (2019), version 5.7.1, National Institute of Standards and Technology, Gaithersburg, MD. Accessed online in June 2020 at https://physics.nist.gov/asd.

[31] E. U. Condon and G. H. Shortley, *The Theory of Atomic Spectra*, reprint ed. (Cambridge University Press, Cambridge, UK, 1957).

[32] V. V. Tsyganok, D. A. Pershin, E. T. Davletov, V. A. Khlebnikov, and A. V. Akimov, Scalar, tensor, and vector polarizability of Tm atoms in a 532-nm dipole trap, Phys. Rev. A **100**, 042502 (2019).

[33] J. Dalibard, Introduction to the physics of artificial gauge fields, in Quantum matter at ultralow temperatures, *Proceedings of the International School of Physics "Enrico Fermi,"* Vol. 191, edited by M. Inguscio, W. Ketterle, S. Stringari, and G. Roati (IOS Press, Amsterdam, 2016), p. 1.

[34] D. Babik, R. Roell, D. Helten, M. Fleischhauer, and M. Weitz, Synthetic magnetic fields for cold erbium atoms, Phys. Rev. A **101**, 053603 (2020).

[35] Yu. Kagan, I. A. Vartan'yants, and G. V. Shlyapnikov, Decay kinetics of the metastable gas-phase of polarized atomic-hydrogen at low-temperatures, Zh. Eksp. Teor. Fiz. **81**, 1113 (1981).

[36] G. V. Shlyapnikov, J. T. M. Walraven, U. M. Rahmanov, and M. W. Reynolds, Decay Kinetics and Bose Condensation in a Gas of Spin-Polarized Triplet Helium, Phys. Rev. Lett. **73**, 3247 (1994).

[37] S. Hensler, J. Werner, A. Griesmaier, P. O. Schmidt, A. Görlitz, T. Pfau, S. Giovanazzi, and K. Rzażewski, Dipolar relaxation in an ultra-cold gas of magnetically trapped chromium atoms, Appl. Phys. B **77**, 765 (2003).

[38] T. Karman, X. Chu, and G. C. Groenenboom, Cold magnetically trapped ^{2}D g scandium atoms. I. Interaction potential, Phys. Rev. A **90**, 052701 (2014).

[39] T. Karman and G. C. Groenenboom, Cold magnetically trapped ^{2}D g scandium atoms. II. Scattering dynamics, Phys. Rev. A **90**, 052702 (2014).

[40] M.-J. Lu, V. Singh, and J. D. Weinstein, Inelastic titanium-titanium collisions, Phys. Rev. A **79**, 050702(R) (2009).

[41] C. V. Ciobanu, S.-K. Yip, and T.-L. Ho, Phase diagrams of $F = 2$ spinor Bose-Einstein condensates, Phys. Rev. A **61**, 033607 (2000).

[42] M. Koashi and M. Ueda, Exact Eigenstates and Magnetic Response of $F = 1$ and $F = 2$ Bose-Einstein Condensates, Phys. Rev. Lett. **84**, 1066 (2000).

[43] M. Ueda and M. Koashi, Theory of spin-2 Bose-Einstein condensates: Spin correlations, magnetic response, and excitation spectra, Phys. Rev. A **65**, 063602 (2002).

[44] H. Makela, Y. Zhang, and K. A. Suominen, Topological defects in spinor condensates, J. Phys. A: Math. Gen. **36**, 8555 (2003).

[45] G. W. Semenoff and F. Zhou, Discrete Symmetries and 1/3-Quantum Vortices in Condensates of $F = 2$ Cold Atoms, Phys. Rev. Lett. **98**, 100401 (2007).

[46] J. L. Song, G. W. Semenoff, and F. Zhou, Uniaxial and Biaxial Spin Nematic Phases Induced by Quantum Fluctuations, Phys. Rev. Lett. **98**, 160408 (2007).

[47] M. Kobayashi, Y. Kawaguchi, M. Nitta, and M. Ueda, Collision Dynamics and Rung Formation of Non-Abelian Vortices, Phys. Rev. Lett. **103**, 115301 (2009).

[48] N. Read and D. Green, Paired states of fermions in two dimensions with breaking of parity and time-reversal symmetries and the fractional quantum Hall effect, Phys. Rev. B **61**, 10267 (2000).

[49] D. A. Ivanov, Non-Abelian Statistics of Half-Quantum Vortices in p-Wave Superconductors, Phys. Rev. Lett. **86**, 268 (2001).

[50] L. Fu and C. L. Kane, Superconducting Proximity Effect and Majorana Fermions at the Surface of a Topological Insulator, Phys. Rev. Lett. **100**, 096407 (2008).

[51] A. Y. Kitaev, Fault-tolerant quantum computation by anyons, Ann. Phys. **303**, 2 (2003).

[52] A. Stern, Anyons and the quantum Hall effect—A pedagogical review, Ann. Phys. **323**, 204 (2008).

[53] C. Nayak, S. H. Simon, A. Stern, M. Freedman, and S. Das Sarma, Non-Abelian anyons and topological quantum computation, Rev. Mod. Phys. **80**, 1083 (2008).

[54] T. Kurosu and F. Shimizu, Laser cooling and trapping of calcium and strontium, Jpn. J. Appl. Phys., Part 2 **29**, L2127 (1990).

[55] T. Kisters, K. Zeiske, F. Riehle, and J. Helmcke, High-resolution spectroscopy with laser-cooled and trapped calcium atoms, Appl. Phys. B **59**, 89 (1994).

[56] C. Oates, F. Bondu, R. Fox, and L. Hollberg, A diode-laser optical frequency standard based on laser-cooled Ca atoms: Sub-kilohertz spectroscopy by optical shelving detection, Eur. Phys. J. D **7**, 449 (1999).

[57] H. Katori, T. Ido, Y. Isoya, and M. Kuwata-Gonokami, Magneto-Optical Trapping and Cooling of Strontium Atoms

Down to the Photon Recoil Temperature, Phys. Rev. Lett. **82**, 1116 (1999).

[58] K. R. Vogel, T. P. Dinneen, A. Gallagher, and J. L. Hall, Narrow-line Doppler cooling of strontium to the recoil limit, IEEE Trans. Instrum. Meas. **48**, 618 (1999).

[59] T. Binnewies, G. Wilpers, U. Sterr, F. Riehle, J. Helmcke, T. E. Mehlstäubler, E. M. Rasel, and W. Ertmer, Doppler Cooling and Trapping on Forbidden Transitions, Phys. Rev. Lett. **87**, 123002 (2001).

[60] T. Kuwamoto, K. Honda, Y. Takahashi, and T. Yabuzaki, Magneto-optical trapping of Yb atoms using an intercombination transition, Phys. Rev. A **60**, R745 (1999).

[61] A. Frisch, K. Aikawa, M. Mark, A. Rietzler, J. Schindler, E. Zupanic, R. Grimm, and F. Ferlaino, Narrow-line magneto-optical trap for erbium, Phys. Rev. A **85**, 051401 (2012).

[62] N. Huet, M. Pettens, and T. Bastin, Isotope shifts and hyperfine structure of the laser-cooling Fe I 358-nm line, Phys. Rev. A **92**, 052507 (2015).

[63] J. C. Berengut, D. Budker, C. Delaunay, V. V. Flambaum, C. Frugiuele, E. Fuchs, C. Grojean, R. Harnik, R. Ozeri, G. Perez, and Y. Soreq, Probing New Long-Range Interactions by Isotope Shift Spectroscopy, Phys. Rev. Lett. **120**, 091801 (2018).

[64] Z. Ben Ahmed, Extension de l'etude du spectre d'arc du scandium: II. Interprétation théorique, Physica B+C **92**, 122 (1977).

[65] J. E. Lawler and J. T. Dakin, Absolute transition probabilities in Sc I and Sc II, J. Opt. Sci. Am. B **6**, 1457 (1989).

[66] W. F. Meggers, C. H. Corliss, and B. F. Scribner, *Tables of Spectral-Line Intensites: Part I—Arranged by Elements*, 2nd ed. (U.S. Department of Commerce, National Bureau of Standards, Washington, D.C., 1975).

[67] P. Hannaford, R. Lowe, G. Nicolas, E. Biemont, and W. Whaling, Oscillator strengths for Y I and Y II and the solar abundance of yttrium, Astrophys. J. **261**, 736 (1982).

[68] J. Flemming, A. M. Tuboy, D. M. B. P. Milori, L. G. Marcassa, S. C. Zilio, and V. S. Bagnato, Magneto-optical trap for sodium atoms operating on the D_1 line, Opt. Commun. **135**, 269 (1997).

[69] B. A. Palmer, The first spectrum of yttrium and an automatic comparator for its measurement, Ph.D. thesis, Purdue University, 1977.

[70] E. A. D. Hartog, A. J. Palmer, and J. E. Lawler, Radiative lifetimes and transition probabilities of neutral lanthanum, J. Phys. B: At., Mol. Opt. Phys. **48**, 155001 (2015).